Differential Tomography: A New Framework for SAR Interferometry

Fabrizio Lombardini, *Senior Member, IEEE*

***Abstract*—In this paper, a new interferometric mode crossing the differential synthetic aperture radar (SAR) interferometry and multibaseline SAR tomography concepts, that can be termed differential SAR tomography, is proposed. Its potentials, coming from the joint elevation-velocity resolution capability of multiple scatterers, are discussed. Processing is cast in a bidimensional baseline-time spectral analysis framework, with sparse sampling. The use of a modern data-dependent bidimensional spectral estimator is proposed for joint baseline-time processing. Simulated results are reported for different baseline-time acquisition patterns and two motion conditions of layover scatterers, showing that this new challenging interferometric technique is promising.**

***Index Terms*—Electromagnetic tomography, multidimensional signal processing, spectral analysis, synthetic aperture radar (SAR) interferometry.**

I. Introduction

DIFFERENTIAL synthetic aperture radar interferometry (D-InSAR) and three-dimensional (3-D) SAR tomography (Tomo-SAR) are two advanced operation modes of SAR interferometry (InSAR). The former is a quite mature InSAR technique: it is based on multiple-pass satellite SAR acquisitions to accurately measure terrain displacements (scatterer velocity); see [1]–[5] and references therein. It can be considered a long-term Doppler technique. It has been long investigated by the scientific community and is now in an operational status, yet there is still room for improvements. Limitations of the standard D-InSAR approach are mainly due to possible atmospheric phase artifacts and temporal and baseline decorrelation. These problems can be overcome by investigation of long time series [4], [5] and proper processing of data from stable ("permanent") scatterers (PS) [4] or from multiple short-baseline (SBAS) track subsets [5]. D-InSAR is fruitfully applied for detecting and mapping centimeter-scale deformations of the ground and monitoring buildings, glacier flows, and slope instabilities. Even millimeter-scale accuracy can be achieved, especially by the PS approach. An overview of D-InSAR applications is given in [6]. Recently, the technique of D-InSAR has been experimented also with airborne data, e.g., see [7], where the challenge is accurate motion compensation.

Tomo-SAR is a more recent InSAR technique: it is based on multibaseline acquisition to produce full 3-D imaging for analysis of semitransparent scattering layers or layover areas; see [8]–[12] and references therein. It is an elevation beamforming technique, and it represents a very promising extension of classical interferometry for topographic mapping. It is still in the experimental stage. A limitation of the Tomo-SAR technique is the typically irregular baseline sampling, which results in a distorted point spread function of elevation imaging. This problem is currently addressed by simple array interpolation (baseline filling) under the assumption of a single dominant elevation scatterer [10], [13] or by regularized inversion [11]. Tomo-SAR can be used to improve the inversion of geophysical parameters of volumetric targets. In particular, it can be an interesting tool for applications involving estimation of forest biomass and height, ground topography, soil humidity, and ice thickness [10], and for solving InSAR height and reflectivity misinterpretation caused by layover geometries in natural or urban areas [12], [13]. Both D-InSAR and Tomo-SAR are applied to stripmap data. Recently, the InSAR technique has been applied also to the case of large-swath burst-mode ScanSAR data; see [14] and references therein.

In this paper, a new interferometric mode crossing the differential SAR interferometry and SAR tomography concepts, which can be termed *differential SAR tomography*, is presented. It allows joint resolution capability of multiple scatterer velocities and elevations in a same range-azimuth cell. Also, an original casting is given of the novel parameter extraction problems in a bidimensional space (baseline)-time spectral analysis framework. This constitutes an extension of the space (range-azimuth)-baseline-time phase-only single-component D-InSAR processing concept in [4] and of the D-InSAR scatterer separation concept in [15]. The potentials of differential SAR tomography are discussed, and case studies of simulated performance analysis are reported.

The rest of the paper is organized as follows. The conceptual description of the new powerful unified framework is given in Section II. The data acquisition modes for differential SAR tomography, which include the plain multibaseline acquisition obtained by multiple passes, are described. The processing challenges of the new interferometric technique are discussed, and a theory for differential tomography is formalized in Section III. The use of a modern flexible bidimensional spectral estimator for irregular data [16], [17] is proposed for joint baseline-time processing. First tests with simulated case studies are presented in Section IV for different baseline-time acquisition patterns and two motion conditions of layover scatterers. Section V reports conclusions and suggestions for future work and potential applications.

Manuscript received August 27, 2003; revised July 23, 2004. Part of this work was presented at IGARSS 2003.

The author is with the Department of Information Engineering, University of Pisa, 56122 Pisa, Italy (e-mail: f.lombardini@iet.unipi.it).

Digital Object Identifier 10.1109/TGRS.2004.838371

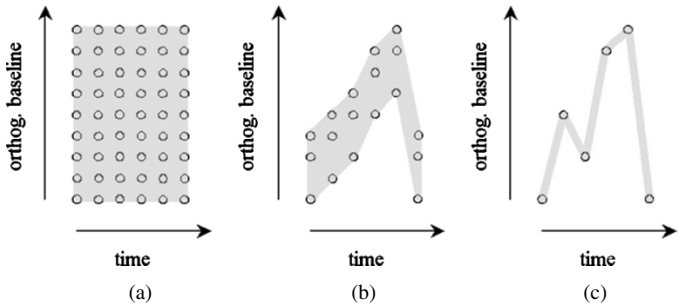

Fig. 1. Data acquisition modes for differential SAR tomography.

II. Differential SAR Tomography Concept

In this section, the acquisition patterns and the processing framework for differential tomography are illustrated. Three jointly multibaseline multitime lag acquisition patterns are considered. As shown in Fig. 1, the acquistion should be multiple-pass, as mandatory in differential interferometry, but with either multibaseline (or, if you like, tomographic) data (a, b), single-baseline InSAR data, or single-channel SAR (c) data acquired for each pass. The only light acquisition constraint, which can be typically met even by plain repeat-pass single-channel SAR, is to cover, even though only sparsely, a two-dimensional (2-D) support in the 2-D baseline-time plane. After registration of the multiple SAR images, and compensation of possible atmospheric phase artifacts [4], [5] and local phase aligning (deramping) [10], [11], consider the complex baseline-time data for a given range-azimuth resolution cell. The multibaseline multitime lag acquisition acts as a bidimensional array device (sparsely) sampling the incoming signal wavefront from the given cell in space and time, after SAR processing. Proper baseline-time bidimensional spectral analysis would then extract *joint* information on scatterer power elevation and Doppler shift (velocity) *distributions* for the given cell, which is a novel interferometric product.

This unified framework can constitute a significant extension of Tomo-SAR, where the temporal dimension is neglected, and of D-InSAR, where only a single (possibly mean) elevation is extracted in conjunction with displacement measurements. With reference to this latter technique, differential tomography can represent an extension of the D-InSAR scatterer separation concept in [15]. There, (phase-only) model matching is investigated for the specific case of just two layover point-like scatterers with the same velocity. The proposed differential tomography framework is more general, in that it can be applied to a larger number of any signal components, possibly with *continuous* elevation-Doppler power distributions (extended and/or time-decorrelating scatterers). Also, it has a richer output (elevation-Doppler *distribution* instead of *parameter* estimates), and it includes the case (b) of single- or multiple-baseline data at each pass. Finally, it potentially allows a wider range of applications than the particular method in [15], as it is hinted in the concluding section.

For many regularly spaced baselines and acquisition times, which is a reference academic case [Fig. 1(a)], plain 2-D-Fourier analysis can provide satisfactory elevation-Doppler resolution and 2-D sidelobe behavior for differential tomography. However, in practice, only one or a few baselines per each pass can be considered [Fig. 1(b)], e.g., from single-baseline or advanced three-antenna airborne systems [18], [19] or from future multistatic satellite clusters [20]. This would realize a *sparse bidimensional* sampling of the 2-D baseline-time plane. With the many current airborne or spaceborne single-channel SAR systems, the acquisition in the baseline-time plane can be considered to be *monodimensional curvilinear*, nevertheless still partially filling the 2-D acquisition space; see the example in Fig. 1(c). For the latter two conditions, classical 2-D spectral analysis would produce untolerable 2-D side- or quasi-grating lobes in the estimated elevation-velocity profiles, as quantified in Section IV. An additional difficulty comes from the fact that practical sparse acquisition patterns of the kind in Fig. 1(b)–(c) typically do not lay on a regular grid (noninteger sampling). A solution to these estimation problems is proposed in next section.

III. Theory of Differential SAR Tomography

A. Problem Statement

The differential tomography concept is formalized as follows. Consider the processing of calibrated baseline-time data from N_P passes, with $N_C \geq 1$ complex SAR images acquired simultaneously at each pass by a possibly single- or multiple-baseline N_C-phase center system, e.g., $N_P = 6$ and $N_C = 3, 1$ in Fig. 1(b) and (c), respectively. Let $B_\perp(u,v), u = 1,\ldots,N_C, v = 1,\ldots,N_P$, be the orthogonal baseline of the uth two-way phase center in the vth pass, with respect to the master acquisition (say, the first phase center in the first pass, thus $B_\perp(1,1) = 0$). Let $t(v), v = 1,\ldots,N_P$, be the acquisition time of the phase centers in the vth pass, with respect to the master acquisition ($t(1) = 0$). As usual in SAR interferometry, in each complex SAR image we consider N independent and identically distributed looks to reduce statistical variations, e.g., multiple homogeneous adjacent pixels (spatial multilooking) or multiple observations obtained by partitioning the synthetic aperture (subaperture multilooking). For each nth look, $n = 1,\ldots,N$, the complex amplitudes of the pixels observed in the $N_C \cdot N_P$ SAR images at a given range-azimuth cell are arranged in the $N_C \times N_P$ baseline-time data matrix $\mathbf{Y}(n)$, where each column collects the (multibaseline) data at each pass. The signal from the scatterers in the given range-azimuth cell is characterized by a bidimensional spatial-temporal spectrum, depending both on the (time-averaged) backscattered power as a function of elevation and the temporal changes of the complex signal contributions from the various elevations.

The problem of the production of an elevation-velocity (*tomo-Doppler*) image for the given range-azimuth cell can be cast as the estimation of the backscattered signal power spatial-temporal spectrum $S(\omega_S, \omega_T)$ from the baseline-time multilook data $\mathbf{Y}(n), n = 1,\ldots,N$. Term ω_S is the spatial frequency, related to the normal to slant range elevation component h_{nsr} as $\omega_S = 4\pi h_{\mathrm{nsr}}/(\lambda r)$, with λ the radar wavelength and r the slant-range distance [10], [12]. Term ω_T is the temporal frequency; when the temporal change of a complex backscatter component is originated by a uniform motion, ω_T is related to the line-of-sight velocity component V_{los} as $\omega_T = 4\pi V_{\mathrm{los}}/\lambda$ [4]. An estimator of $S(\omega_S, \omega_T)$ is proposed in the sequel.

B. Differential Tomographic Processor

To deal with the difficult baseline-time spectral analysis problem of differential SAR tomography, in this paper it is proposed to resort to the emerging class of adaptive filterbank methods for 2-D spectral analysis, which can effectively handle also 2-D sparse or gapped data [16], [17]. These methods do not exploit any *a priori* assumption on the 2-D spectrum (in differential tomography, the elevation-Doppler power distribution). Yet, they can largely outperform Fourier methods (the gain depending on the particular baseline-time acquisition pattern, the signal-to-noise ratio (SNR), and the 2-D spectrum shape). In particular, the shape of the bidimensional frequency response of the 2-D-Capon filter [16], [21] adaptively changes during the bidimensional spectral scan, depending on the input data. This allows to reject interference coming from noise and signal components at other bidimensional frequencies than the selected, through setting of data-dependent 2-D nulls. As a result, improvement in terms of both leakage level and resolution is obtained (note that the overall filtering process is nonlinear [16]).

In the differential tomography framework, consider the $N_C \times N_P$ baseline-time *steering matrix* $\mathbf{A}(\omega_S, \omega_T)$, coding the response of the bidimensional baseline-time (sparse) array to a backscattered signal component with spatial and temporal frequencies ω_S, ω_T

$$\mathbf{A}(\omega_S,\omega_T) = \begin{bmatrix} 1 & \cdots & e^{j[\omega_S B_\perp(1,N_P)+\omega_T t(N_P)]} \\ \vdots & \vdots\vdots & \vdots \\ e^{j\omega_S B_\perp(N_C,1)} & \cdots & e^{j[\omega_S B_\perp(N_C,N_P)+\omega_T t(N_P)]} \end{bmatrix}. \quad (1)$$

Let $\mathbf{a}(\omega_S, \omega_T)$ be the $(N_C \cdot N_P) \times 1$ baseline-time steering vector and $\mathbf{y}(n)$ the $(N_C \cdot N_P) \times 1$ baseline-time data vector

$$\mathbf{a}(\omega_S,\omega_T) = \mathrm{vec}[\mathbf{A}(\omega_S,\omega_T)], \qquad \mathbf{y}(n) = \mathrm{vec}[\mathbf{Y}(n)], \quad (2)$$

where $\mathrm{vec}[\,\cdot\,]$ is the vec-operator which stacks the columns of the matrix between parenthesis. A data-dependent $(N_C \cdot N_P) \times 1$ vector of spatial-temporal filtering coefficients $\mathbf{h}(\omega_S, \omega_T)$ is designed with closed-form solution, that passes the signal component with frequencies ω_S, ω_T in $\mathbf{y}(n)$ without distortion and, at the same time, attenuates all the other signal components as much as possible. From the filter output, the 2-D-Capon-estimated [16], [17] tomo-Doppler power image is obtained as

$$\hat{P}_C(\omega_S,\omega_T) = 1 \Big/ \left[\mathbf{a}^H(\omega_S,\omega_T)\hat{\mathbf{R}}_y^{-1}\mathbf{a}(\omega_S,\omega_T)\right] \quad (3)$$

where $(\,\cdot\,)^H$ denotes conjugate transpose, and the $(N_C \cdot N_P) \times (N_C \cdot N_P)$ matrix $\hat{\mathbf{R}}_y$ is a multilook estimate of the baseline-time data vector covariance matrix. For the sake of simplicity, the scaling to produce a true power spectral density estimate $\hat{S}(\omega_S, \omega_T)$ is not included in (3). Since in general the baseline-time sampling is sparse, the unstructured sample covariance matrix estimate $\hat{\mathbf{R}}_y = N^{-1}\sum_{n=1}^{N}\mathbf{y}(n)\mathbf{y}^H(n)$ is employed, with $N \geq N_C \cdot N_P$ for $\hat{\mathbf{R}}_y$ to be positive definite [17].

IV. Simulated Case Studies

To get a flavor of the potential performance of differential tomography, simulated results are reported. Various spatial (elevation) spectrum models can be considered, for specific surface types possibly accounting for volume scattering [22] [10] and layover [18], [12]. Modeling of the temporal spectrum is a more difficult task. Phase changes are originated by a global motion component of each backscattering source in the range-azimuth cell. In addition to that, both amplitude and phase of the corresponding component of radar backscatter can be perturbed by changes of relative geometry of the source scatterers in the resolution cell (internal motion) and by changes of dielectric constant, arising from different phenomena [23], [24]. Moreover, at the best of the author's knowledge, models of joint spatial (elevation)-temporal spectra of interferometric signals are not available in the literature. Thus, two simple models of the spatial-temporal spectrum of multiple signal components are considered in this paper for simulated analysis of differential tomography. It is worth stressing that the 2-D-Capon filter does not exploit any information on these models: it is a nonparametric spectral estimator as the Fourier methods. This performance analysis is by no means exhaustive and is not targeted to a specific surface type for a particular application. It is reported as a guide to identify the basic potentials of the new technique and the acquisition pattern and signal properties that most influence the achievable performance. In particular, two motion conditions of layover scatterers are considered: uniform motion and uniform motion affected by velocity jitter.

A. Uniform Motion

Consider the curvilinear baseline-time acquisition pattern in Fig. 1(c), with $N_P = 6$ passes of a single-channel SAR ($N_C = 1$), obtained by thinning the filled $(N_P = 6) \times (N_C = 9)$ uniform acquisition pattern in Fig. 1(a). $N = 32$ looks of the corresponding baseline-time data are generated. In this first set of simulations, the bidimensional spatial-temporal spectrum considered is discrete and consists of two 2-D line components at frequencies $(\omega_{Si}, \omega_{Ti}) = (0, 0)$ and $(1.5, 1)$, where ω_{Si} and ω_{Ti} are normalized spatial and temporal frequencies in Rayleigh (elevation) and Fourier (Doppler) resolution units, respectively. The signal-to-thermal-noise ratio (SNR) for the two components in isolation is 15 and 12 dB, respectively. Each signal component has circular Gaussian complex amplitude, fluctuating from look to look. This simple scenario can model two layovered bunches of scatterers, the first steady and the second in uniform motion (constant velocity). Each bunch of scatterers has a small spread along the normal to slant range elevation axis; thus, baseline and volumetric decorrelation effects are negligible [4], [12], [22], and there is neither significant internal motion nor changes of complex reflectivity with time [23].

A realization of a Fourier-based tomo-Doppler power image is shown in Fig. 2. It is produced by the multilook 2-D periodogram (2-D beamforming) [17], [21]

$$\hat{P}_B(\omega_S,\omega_T) = \mathbf{a}^H(\omega_S,\omega_T)\hat{\mathbf{R}}_y\mathbf{a}(\omega_S,\omega_T)/(N_C N_P)^2 \quad (4)$$

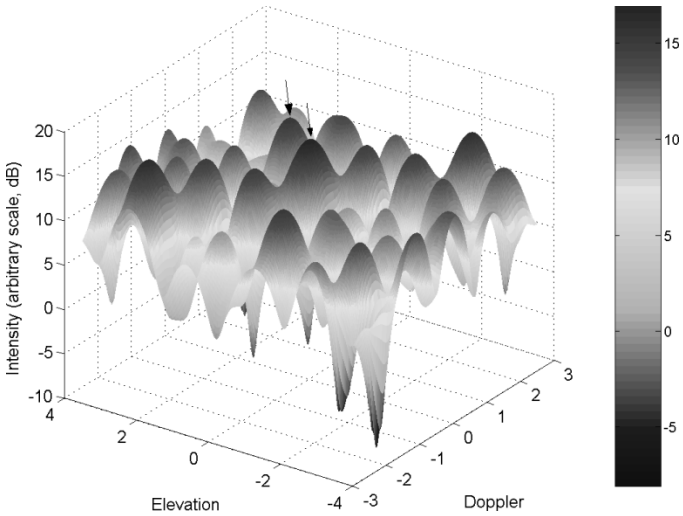

Fig. 2. Two-dimensional-Fourier-based tomo-Doppler image, curvilinear pattern.

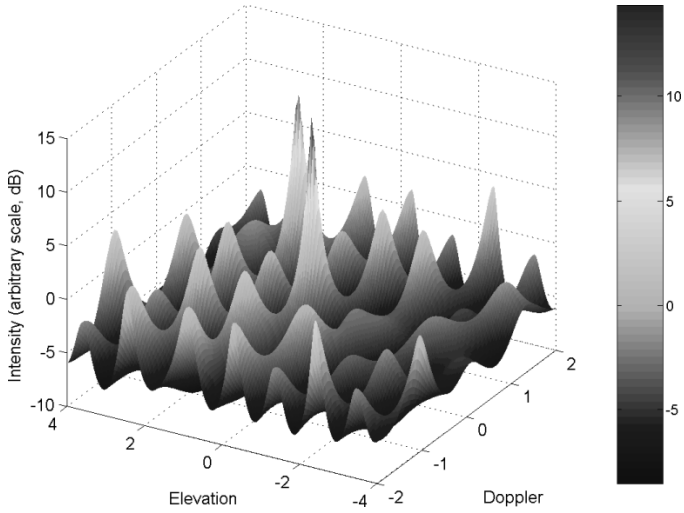

Fig. 4. Two-dimensional-Capon-based tomo-Doppler image, curvilinear pattern, $N_P = 5$.

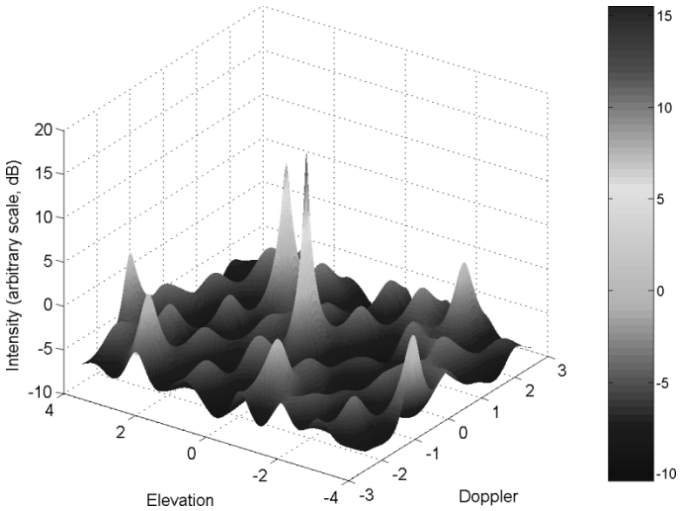

Fig. 3. Two-dimensional-Capon-based tomo-Doppler image, curvilinear pattern.

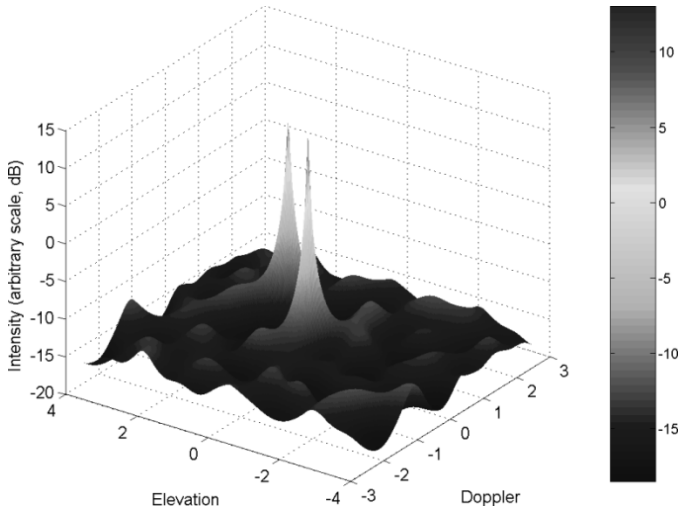

Fig. 5. Two-dimensional-Capon-based tomo-Doppler image, sparse 2-D pattern.

with ω_S, ω_T (if you wish, h_{nsr} and V_{los}) reported in Rayleigh and Fourier resolution units, respectively, over the unambiguous estimation range. It can be seen that the curvilinear acquisition is enough to get joint elevation-Doppler resolution of the two signal components, since it covers a 2-D support in the baseline-time plane. The spectral peaks corresponding to the signal components are marked by the arrows. However, it is apparent how the Fourier estimated tomo-Doppler image is impaired by untolerable 2-D sidelobes because of the very sparse acquisition pattern. To quantify this effect, the level of the mainlobes corresponding to the signal components and the level of the peak sidelobe have been measured. The peak sidelobe level (PSL) normalized by the height of the first component mainlobe is only -1 dB. The PSL normalized by the second component mainlobe height is even larger than one ($+1$ dB), i.e., the second component is masked. A realization of the 2-D-Capon-estimated tomo-Doppler power image (3) is shown in Fig. 3. Notably, the proposed Capon tomo-Doppler processor exhibits much better sidelobe behavior thanks to the adaptive rejection of leakage, together with resolution beyond the Rayleigh/Fourier limits. The PSL normalized by the first and second component mainlobes has now the reasonable value -13 and -8 dB, respectively.

To show how significant can be the effect of the pattern of acquisition on the achievable performance, an even more critical curvilinear pattern with only $N_P = 5$ passes is considered, which is obtained by dropping the second pass $(v = 2)$ in the pattern in Fig. 1(c). Capon tomo-Doppler imaging still outperforms Fourier (not shown here), but the achieved sidelobe level is less satisfactory than before; see Fig. 4 (Fourier normalized PSLs -0.5 and $+4$ dB, -10 and -7 dB for Capon). Conversely, the more dense acquisition pattern of Fig. 1(b), achievable by simultaneous multibaseline acquisition $(N_C = 3)$ at each pass, results in the very good Capon tomo-Doppler image in Fig. 5 (normalized PSLs -23 and -21 dB, versus -4.5 and -1.5 dB of Fourier imaging, not shown here).

A realistic scenario of curvilinear baseline-time acquisition with noninteger baseline sampling is also considered, assuming the baseline values of the ERS-1 Bonn dataset with three days revisit time ($N_P = 10$ passes). The orthogonal baseline lengths with respect to the master acquisition are $B_\perp(1, v) = 0, 601, 1174, 1382, 1214, 853, 427, 1153, 1418,$

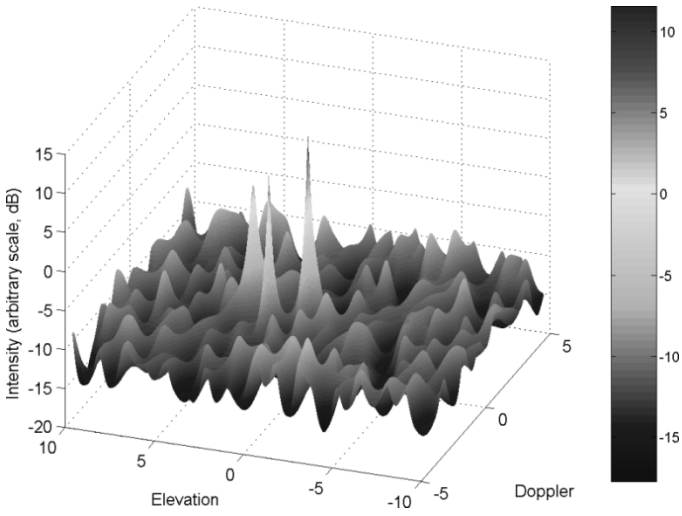

Fig. 6. Two-dimensional-Capon-based tomo-Doppler image, Bonn pattern.

and 1322 m, for $v = 1, \ldots, 10$, respectively. A slightly more complex spatial-temporal spectrum is now considered, with three line components at normalized frequencies $(\omega_{Si}, \omega_{Ti}) = (0,0), (1.5, -1)$, and $(3,0)$, with SNRs 15, 12, and 9 dB, respectively. This models three layover bunches of scatterers; the one at the middle elevation is moving, and the other two are steady. A realization of the corresponding simulated Capon tomo-Doppler image, with a lower number of looks $N = 16$, is reported in Fig. 6 (only portion of the elevation axis is shown). It exhibits both good resolution and reasonable sidelobe level. The PSL normalized by the three components mainlobes is -16.5, -12.5, and -9.5 dB, respectively. In other simulations not shown here, resolution beyond the Rayleigh/Fourier limits and similar sidelobe levels have been obtained for normalized intersource elevation/Doppler separation down to 0.5 and 0.1, respectively.

B. Jittered Motion

In the second set of simulations, motion jitter is included, which perturbs the uniform motion. The case of a displacement component statistically independent between different acquisition times, which is superimposed to the constant velocity component, is considered. Line-of-sight displacement perturbations are assumed to be Gaussian distributed, with zero mean and standard deviation σ_d. A few considerations are in order for this simulation model. Independent motion jitter has been assumed, since it is the worst case in terms of spectral spreading. In fact, the independent displacement component produces for the signal backscattered from the jittered source in isolation the normalized temporal autocorrelation function

$$\rho(\Delta v) = \begin{cases} e^{-(4\pi\sigma_d/\lambda)^2}, & \text{for } \Delta v = v_1 - v_2 \neq 0 \\ 1, & \text{for } \Delta v = 0 \end{cases} \quad (5)$$

where v_1 and v_2 are two pass indexes (steady temporal decorrelation) [23], [25]. By virtue of the Wiener–Khintchine theorem, this corresponds to a mixed line-continuous constant Doppler spectrum. Thus, independent jitter results in the discrete 2-D spectral line of Section IV-A being buried in a constant spectral floor spread all over the Doppler unambiguous range, localized at the elevation of the bunch of scatterers affected by jitter (this 2-D spectral component associated to jitter can be called semidiscrete). Time-correlated jitter, or volumetric effects, would generally result in more limited spectral spread (along the Doppler or elevation dimension, respectively). Thus, the case of independent jitter can give a good flavor of possible performance loss in critical real-world conditions. In fact, it is expected that performance of differential tomography tends to reduce in presence of spectral spreads. However, it is known that Capon spectral estimators behave better than or equal to the periodogram in terms of resolution and sidelobes [21, ch. 6], even when nonline spectra are considered (e.g., see [26] for a monodimensional interferometric case). This is because of the adaptive maximal leakage rejection of Capon estimator. For spectra tending to be completely flat, the adaptive Capon estimator has no more degrees of freedom to place proper nulls in the frequency response, and it tends exactly to the periodogram [21, ch. 6]. Thus, one should expect reduced performance of Capon-based differential tomography in case of independent jitter leading to Doppler-spreaded spectral components, yet no reversed ranking compared to the periodogram.

Concerning the multiple data looks, two extreme conditions are considered in this paper for the jitter: same history of motion jitter for all the N looks and statistically independent motion jitter history for each look. In the first model, jitter realizations are completely correlated among the looks. We refer to this condition as the correlated jitter case. Correlated jitter can arise when subaperture multilooking is employed. In this case, the looks correspond to the same range-azimuth resolution cell; thus, the jitter observed at a given acquisition time $t(v), v = 1, \ldots, N_P$, is the same for all $n = 1, \ldots, N$. Conversely, when spatial multilooking is adopted, jitter realizations would be generally only partially correlated among the looks. In fact, it is expected that the jitter values observed at a given acquisition time $t(v)$ for different pixels exhibit various degrees of similarity, according to the distance between the pixels and the degree of spatial nonhomogeneity of the physical source of motion jitter. In this paper, for the sake of simplicity, we consider as second jitter model that of jitter completely uncorrelated among the N pixels (looks). We refer to this condition as the independent jitter case. The extreme case of independent jitter, coupled with the correlated jitter model, is useful to investigate the range of achievable performance in presence of partially correlated jitter from spatial multilooking. As already stated, in both models jitter samples are independent in time. Where not otherwise explicitly stated, the adjective independent/correlated refers to the look statistical condition, not to the time one.

A realization of Capon-based tomo-Doppler imaging in the presence of independent jitter is shown in Fig. 7 for the sparse 2-D acquisition pattern ($N_P = 6, N_C = 3$). Two fluctuating signal components are considered with the same parameters as for Figs. 2–5, and again $N = 32$. The signal source in motion is affected by displacement perturbations with $\sigma_d = 2.5\%$ of λ. It is easily computed that changes of the (mean) line-of-sight velocity $V_{\text{los}}(v)$ between the vth and $(v+1)$th acquisition, $v = 1, \ldots, N_P - 1$, are Gaussian with relative standard deviation $\sigma_{V_{\text{los}}(v)}/V_{\text{los}} = 2\sqrt{2}(N_P - 1)(\sigma_d/\lambda)/\omega_{Ti}$, where V_{los} is the average line of sight velocity, and ω_{Ti} is the

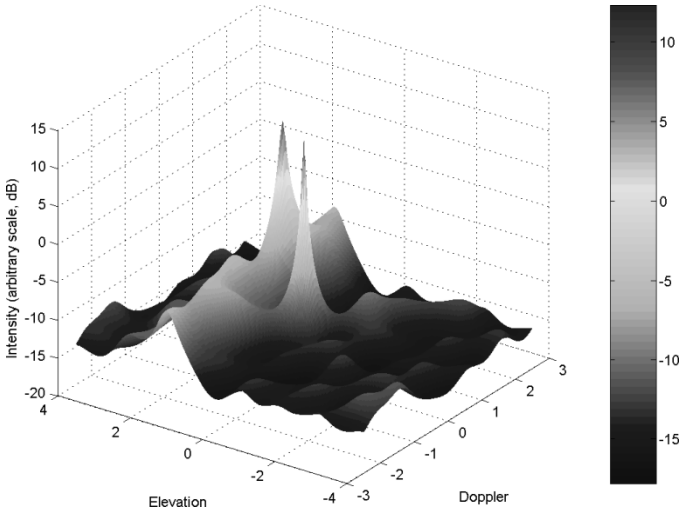

Fig. 7. Two-dimensional-Capon-based tomo-Doppler image, sparse 2-D pattern, independent jitter.

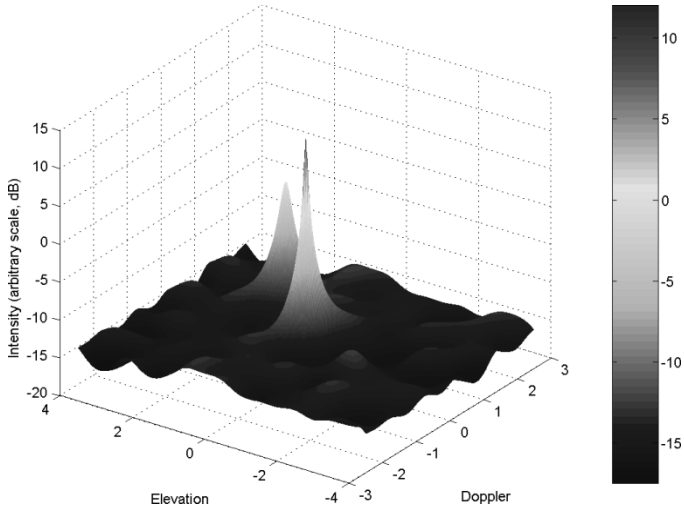

Fig. 8. Two-dimensional-Capon-based tomo-Doppler image, sparse 2-D pattern, correlated jitter.

corresponding temporal frequency expressed in Fourier resolution units. For the parameters of this case study, $\sigma_{V_{\rm los}(v)} = 35\%$ of $V_{\rm los}$. This condition models a monotonic jittered motion, in that the probability of reversed motion is negligible: $P\{V_{\rm los}(v) < 0\} \approx P\{V_{\rm los}(v) - V_{\rm los} < -3\sigma_{V_{\rm los}}(v)\} \approx 0$. The elevation-localized Doppler-constant spectral floor originated by the temporal independent jitter of the moving source is apparent in the estimated tomo-Doppler image. It can be seen that the spectral peaks of the two signal components are well resolved, with just a little sidelobe level increase compared to the corresponding nonjittered scenario of Fig. 5. The PSL normalized by the first and second component mainlobes has the still good value -21 and -18.5 dB, respectively. Here, the PSL has been evaluated discarding the localized spectral floor from jitter, since it is a signal feature, not an imaging artifact. This spectral feature is around 2–4 dB higher than the peak sidelobe.

A tomo-Doppler image for the case of correlated jitter is shown in Fig. 8, with all the parameters set as above. Two peculiarities are easily seen of performance of differential tomography when jitter is present and is completely correlated among the looks. One is that the spectral feature of jitter is not detected, differently from the case of jitter independent from look to look. The second is that the jittered source exhibits an intensity loss in the tomo-Doppler image, while the sidelobe level is very similar to the nonjittered case. The resulting normalized PSLs are -23 and -13 dB, which is still satisfactory despite the 8-dB loss for the jittered source compared to the nonjittered case of Fig. 5. The difficulty of detecting the spectral feature of jitter when it is correlated is due to ergodicity problems. The temporal observation window is too short to allow reliable estimate of ergodic autocorrelation from the single temporal sequence of jitter values common to all the looks.

The effect of jitter on differential interferometry with curvilinear acquisition has also been analyzed. The case of independent jitter from look to look has been considered first. It is expected that curvilinear acquisition cannot detect the spectral feature of jitter even under the favorable condition of jitter independence among the looks. This is due to the fact that time-independent jitter is not identifiable in the 2-D elevation-Doppler spectral domain: as an example, its effect on the observed curvilinear data does not differ from that of a source extended all over the elevation unambiguous range and not affected by jitter. This has been confirmed by simulations assuming again the baseline-time pattern of the Bonn dataset ($N_P = 10$), with the three signal sources and $N = 16$ as in Fig. 6. Independent jitter is assumed for the moving source, with $\sigma_d = 1.25\%$ of λ. This corresponds to $\sigma_{V_{\rm los}(v)} = 32\%$ of $V_{\rm los}$, thus monotonic jittered motion as for the sparse pattern scenario. A realization of Capon tomo-Doppler imaging, not shown here for lack of space, shows that independent jitter tends to slightly increase the sidelobe level, as it happens for the sparse pattern. However, the spectral feature of jitter is not detected now. The PSL normalized by the first, second, and third component mainlobes is $-12, -10.5$, and -8 dB, respectively. Then, the more critical case of correlated jitter has been considered, and a realization of the Capon tomo-Doppler estimator for this scenario is shown in Fig. 9. Sidelobe level is similar to the corresponding nonjittered case of Fig. 6. The normalized PSLs are -14 dB for the stronger steady source, -7.5 dB for the moving source, and -9 dB for the weaker steady source. These are reasonable

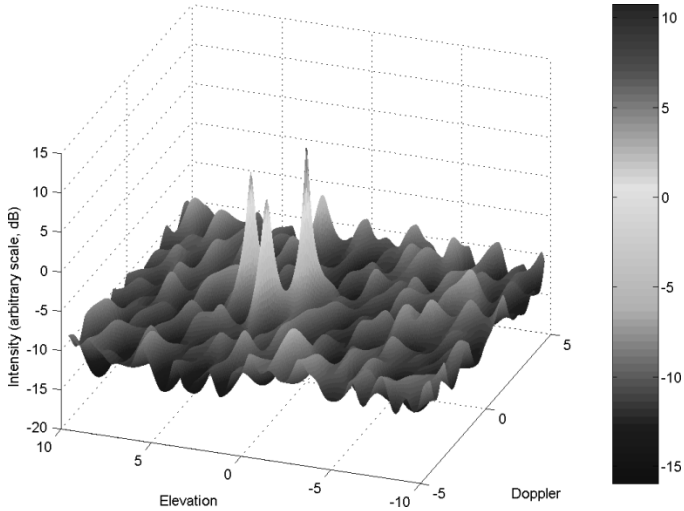

Fig. 9. Two-dimensional-Capon-based tomo-Doppler image, Bonn pattern, correlated jitter.

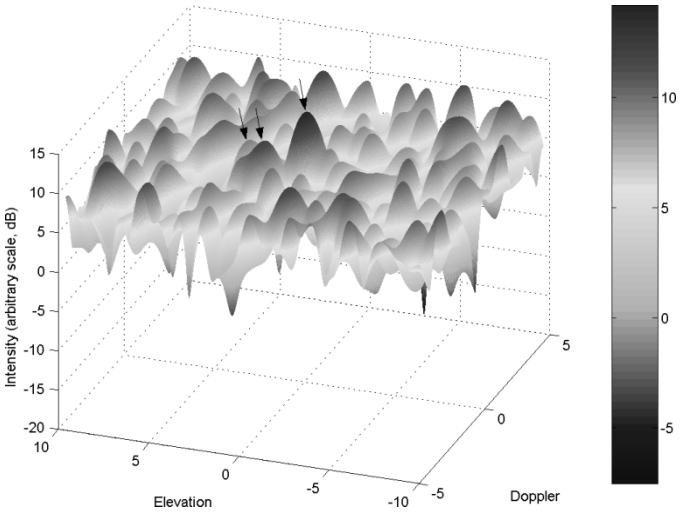

Fig. 10. Two-dimensional-Fourier-based tomo-Doppler image, Bonn pattern, correlated jitter.

values and are quite similar to those of the nonjittered case, except for the source affected by jitter whose estimated intensity has a 5-dB loss.

A realization of Fourier differential tomography for the case of Bonn pattern and correlated jitter is also reported in Fig. 10. It is apparent how Fourier-based tomo-Doppler imaging is still sensibly outperformed by Capon tomo-Doppler imaging, as expected, despite the spectral spread from jitter. This has been observed also for the Fourier tomo-Doppler images of the jittered scenario with sparse pattern, not shown here. The normalized PSLs measured from the Fourier image realization in Fig. 10 are -2, 0, and $+2$ dB, which are by no means acceptable. In particular, the moving source is almost masked, and the weaker steady source is masked by the peak sidelobe, differently from what seen in Fig. 9 (source spectral peaks are marked by the arrows). This confirms the utility of the 2-D-Capon filter proposed for differential tomographic processing, even in presence of a critical real-world condition. In other simulations not shown here, normalized intersource elevation/Doppler separation down to 0.5 and 0.1 has been considered, respectively, with jittered motion still constrained to be monotonic. Resolution of the three sources has been obtained both for independent and correlated jitter with the Capon tomo-Doppler processing of the Bonn pattern data.

As a final comment on the potentials of the new technique, it has to be noted that differential tomography is, in principle, applicable also to ScanSAR interferometric multibaseline data, provided the necessary processing steps specific of ScanSAR interferometry are applied [14]. However, the typically coarse azimuth resolution of burst-mode ScanSAR data could partially limit the potentials that differential tomography would offer for higher resolution (conventional strip-map) interferometric SAR data. In fact, layover sources that are distinct at a single azimuth coordinate could be globally overlapped, and thus possibly separable with more difficulty along the elevation dimension, if azimuth slopes are significant and the azimuth resolution cell is coarse. Also, possible large velocity spreads from nonspatially homogenous terrain displacements in coarse azimuth resolution cells may lower the obtainable accuracy on estimation of (mean) velocity. It has to be recalled that problems from coarse resolution affect also conventional ScanSAR interferometry [14]. However, the functionality of differential tomography with ScanSAR data could be affected to a larger extent by nonhomogeneities, since the useful capabilities of the adaptive Capon filter would tend to be reduced in the presence of significantly spread and strong spectral components. Quantifying also the above-mentioned effects is beyond the goal and space of this paper. Given the increasing interest in ScanSAR techniques, investigation on the possible applicability of the differential tomography concept to ScanSAR interferometry may be worthy of future research.

V. Conclusion

In this paper, the new differential tomography framework has been proposed and formalized. It unifies the differential interferometry an 3-D tomography concepts, allowing for joint elevation-velocity resolution capability. The critical processing aspects arising in this generalized framework have been discussed. The 2-D multilook Capon filterbank has been proposed to process the sparse 2-D or curvilinear baseline-time data. Simulated sample results of joint elevation-Doppler resolution have been reported for a few representative baseline-time acquisition configurations, for simple multiple scattering scenarios with both uniform and jittered motion. The identified performance trends can be summarized as follows. Curvilinear acquisition patterns can be enough to produce tomo-Doppler images, yet a sparse 2-D pattern is beneficial to the sidelobe level. Compared to the case of uniform motion, independent jitter from look to look tends to increase the sidelobe level; jitter completely correlated among the multiple looks tends to produce a source intensity loss. Although the new technique is challenging, simulated results are encouraging, and there is indication that promising performance may be obtained in practical applications.

The work described in this paper represents a beginning of the study of general solutions for, and potentials of, joint elevation-velocity imaging of multiple scatterers. It could serve as a foundation for investigating a few aspects which are left for future research. In some specific situations, other kinds of advanced spectral estimators may also be used for baseline-time processing. Tests with real data are in order. The first performance analysis of the new differential tomography concept reported in this paper is representative, yet further investigation is needed for full performance modeling in actual conditions, with reference to specific surface types for particular applications. In particular, volumetric scattering and temporal reflectivity changes could be included in the performance analysis. The interesting potentials of the new technique can be further investigated to study the feasibility of novel imaging products exploiting joint elevation-Doppler profiling, which may be useful for new environmental monitoring applications. Also, conventional differential interferometry and SAR tomography may sensibly benefit from being cast in the more general framework of differential tomography. Methods could be developed to get improved operation of differential interferometry and SAR

tomography, which cannot satisfactorily operate in the presence of layover [15] and moving scatterers [25], respectively.

ACKNOWLEDGMENT

The author thanks the anonymous reviewers for their constructive comments, which stimulated an extension of the performance analysis in the earlier version of the paper, and for raising the attention to [14].

REFERENCES

[1] A. Gabriel, R. M. Goldstein, and H. A. Zebker, "Mapping small elevation changes over large areas: Differential radar interferometry," *J. Geophys. Res.*, vol. 94, no. B7, pp. 9183–9191, 1989.

[2] D. Massonnet, H. Vadon, and M. Rossi, "Reduction of the need for phase unwrapping in radar interferometry," *IEEE Trans. Geosci. Remote Sensing*, vol. 34, pp. 489–497, Mar. 1996.

[3] I. R. Joughin, R. Kwok, and M. A. Fahnestock, "Interferometric estimation of three-dimensional ice-flow using ascending and descending passes," *IEEE Trans. Geosci. Remote Sensing*, vol. 36, pp. 25–37, Jan. 1998.

[4] A. Ferretti, C. Prati, and F. Rocca, "Nonlinear subsidence rate estimation using permanent scatterers in differential SAR interferometry," *IEEE Trans. Geosci. Remote Sensing*, vol. 38, pp. 2202–2212, Sept. 2000.

[5] P. Berardino, G. Fornaro, R. Lanari, and E. Sansosti, "A new algorithm for surface deformation monitoring based on small baseline differential SAR interferograms," *IEEE Trans. Geosci. Remote Sensing*, vol. 40, pp. 2375–2383, Nov. 2002.

[6] P. A. Rosen, S. Hensley, I. R. Joughin, F. K. Li, S. N. Madsen, E. Rodriguez, and R. M. Goldstein, "Synthetic aperture radar interferometry," *Proc. IEEE*, vol. 88, pp. 333–382, Mar. 2000.

[7] A. Reigber and R. Scheiber, "Airborne differential SAR interferometry: First results at L-band," *IEEE Trans. Geosci. Remote Sensing*, vol. 41, pp. 1516–1520, June 2003.

[8] P. Pasquali, C. Prati, F. Rocca, M. Seymour, J. Fortuny, E. Ohlmer, and A. J. Sieber, "A 3D SAR experiment with EMSL data," in *Proc. IGARSS*, Firenze, Italy, 1995, pp. 784–786.

[9] Z. She, D. A. Gray, R. E. Bogner, and J. Homer, "Three-dimensional SAR imaging via multiple pass processing," in *Proc. IGARSS*, Hamburg, Germany, 1999, pp. 2389–2391.

[10] A. Reigber and A. Moreira, "First demonstration of airborne SAR tomography using multibaseline L-band data," *IEEE Trans. Geosci. Remote Sensing*, vol. 38, pp. 2142–2152, Sept. 2000.

[11] G. Fornaro, F. Serafino, and F. Soldovieri, "Three-dimensional focusing with multipass SAR data," *IEEE Trans. Geosci. Remote Sensing*, vol. 41, pp. 507–517, Mar. 2003.

[12] F. Lombardini, M. Montanari, and F. Gini, "Reflectivity estimation for multibaseline interferometric radar imaging of layover extended sources," *IEEE Trans. Signal Processing*, vol. 51, pp. 1508–1519, June 2003.

[13] G. Fornaro, "Three-dimensional SAR imaging with ERS data," in *Proc. 2003 Tyrrhenian Int. Workshop Remote Sensing*, Elba Island, Italy, 2003, pp. 271–280.

[14] J. Holzner and R. Bamler, "Burst-mode and ScanSAR interferometry," *IEEE Trans. Geosci. Remote Sensing*, vol. 40, pp. 1917–1934, Sept. 2002.

[15] A. Ferretti, C. Prati, and F. Rocca, "Higher order permanent scatterers analysis," presented at the *IGARSS*, Toronto, ON, Canada, 2002.

[16] J. Capon, "High resolution frequency wavenumber spectrum analysis," *Proc. IEEE*, vol. 57, pp. 1408–1418, Aug. 1969.

[17] H. L. Van Trees, *Optimum Array Processing*. New York: Wiley, 2002, vol. 4, Detection, Estimation, and Modulation Theory.

[18] L. Roessing and J. Ender, "Advanced SAR interferometry techniques with AER-II," in *Proc. Int. Radar Symp.*, Munich, Germany, 1998, pp. 1261–1269.

[19] M. Rombach and J. Moreira, "Description and applications of the multipolarized dual band OrbiSAR-1 InSAR sensor," in *Proc. IEEE RADAR Conf.*, Adelaide, Australia, 2003.

[20] G. Krieger, M. Wendler, H. Fiedler, J. Mittermayer, and A. Moreira, "Performance analysis for bistatic interferometric SAR configurations," in *Proc. IGARSS*, Toronto, ON, Canada, 2002, pp. 650–652.

[21] P. Stoica and R. Moses, *Introduction to Spectral Analysis*. Upper Saddle River, NJ: Prentice-Hall, 1997.

[22] E. Rodriguez and J. M. Martin, "Theory and design of interferometric synthetic aperture radars," *Proc. Inst. Elect. Eng., F*, vol. 139, no. 2, pp. 147–159, Apr. 1992.

[23] H. A. Zebker and J. Villasenor, "Decorrelation in interferometric radar echoes," *IEEE Trans. Geosci. Remote Sensing*, vol. 30, pp. 950–959, Sept. 1992.

[24] J. Askne and G. Smith, "Forest InSAR decorrelation and classification properties," in *Proc. Fringe'96—ESA Workshop*, Zurich, Switzerland, 1996, pp. 95–103.

[25] F. Lombardini and H. D. Griffiths, "Effect of temporal decorrelation on 3D SAR imaging using multiple pass beamforming," in *Proc. IEE-EUREL Meeting Radar and Sonar Signal Processing*, Peebles, U.K., 1998, pp. 34/1–34/4.

[26] F. Lombardini, F. Gini, and P. Matteucci, "Application of array processing techniques to multibaseline InSAR for layover solution," in *Proc. 2001 IEEE Radar Conf.*, Atlanta, GA, 2001, pp. 210–215.

Fabrizio Lombardini (M'93–SM'03) received the laurea degree (with honors) in electronic engineering and the Ph.D. degree in telecommunication engineering from the University of Pisa, Pisa, Italy, in 1993 and 1997, respectively.

In 1997, he was granted by the European Union a Marie Curie Fellowship of the Training and Mobility of Researchers (TMR) Program, which he spent as Postdoctoral Researcher with the Department of Electronic and Electrical Engineering, University College London, London, U.K., from 1998 to 1999. Then, he joined the Department of Information Engineering, University of Pisa, where he is currently an Assistant Professor. He has given lectures at universities and institutions in Italy and abroad and has organized one EURASIP journal special issue. He is coauthor of a tutorial entitled "Multibaseline Post-processing for SAR Interferometry," which was presented at the IEEE Sensor Array and Multichannel Workshop (July 2004). His general interests are in the areas of statistical signal processing, estimation, and detection theory, adaptive and superresolution spectral analysis, array processing, and performance bounds evaluation, with application to radar systems. In particular, his research interests include multibaseline and multifrequency interferometric SAR algorithms and systems, both cross- and along-track, multibaseline SAR tomography, multisensor data fusion, and radar detection in non-Gaussian clutter.

Dr. Lombardini has chaired two special sessions at international conferences.